

Voltage-dependent K⁺ channel gating and voltage sensor toxin sensitivity depend on the mechanical state of the lipid membrane

Daniel Schmidt and Roderick MacKinnon¹

Howard Hughes Medical Institute, Laboratory of Molecular Neurobiology and Biophysics, The Rockefeller University, 1230 York Avenue, New York, NY 10021

Contributed by Roderick MacKinnon, October 13, 2008 (sent for review October 3, 2008)

Voltage-dependent K⁺ (Kv) channels underlie action potentials through gating conformational changes that are driven by membrane voltage. In this study of the paddle chimera Kv channel, we demonstrate that the rate of channel opening, the voltage dependence of the open probability, and the maximum achievable open probability depend on the lipid membrane environment. The activity of the voltage sensor toxin VSTx1, which interferes with voltage-dependent gating by partitioning into the membrane and binding to the channel, also depends on the membrane. Membrane environmental factors that influence channel function are divisible into two general categories: lipid compositional and mechanical state. The mechanical state can have a surprisingly large effect on the function of a voltage-dependent K⁺ channel, including its pharmacological interaction with voltage sensor toxins. The dependence of VSTx1 activity on the mechanical state of the membrane leads us to hypothesize that voltage sensor toxins exert their effect by perturbing the interaction forces that exist between the channel and the membrane.

Kv channel | VSTx1 | mechanosensitivity

Several comprehensive studies on the lipid composition of cell membranes have revealed a surprising degree of complexity (1–4). Most membranes are highly heterogeneous and the distribution of lipid and other molecules varies enormously from one membrane type to another. Given this complexity, one cannot help but wonder to what extent the membrane environment determines the function of a membrane protein.

It is well established that the function of certain membrane proteins does depend on the particular lipid composition of a cell membrane. In some cases, protein activity can only be observed in the presence of specific lipid molecules (5–7). In other cases, the membrane can have more subtle effects on the activity of a protein, as if certain kinds of lipids (not necessarily “signaling lipids”) exert a regulatory effect on the membrane protein’s function (8–10).

This study focuses on the membrane dependence of a protein known as a voltage-dependent K⁺ (Kv) channel. Gating (the process of opening and closing) in Kv channels is governed by voltage across the membrane, which means that Kv channels are voltage-dependent switches for turning on ionic currents (11). Kv channels serve many different functions in different cells, but most notably they underlie action potentials in electrically excitable cells, for example in neurons and muscle.

We begin by characterizing the function of the same Kv channel in two different membranes and then address through experiment the origin of distinct behavior imposed by the membrane. We find that the membrane environment exerts profound effects on voltage-dependent gating and on the interaction of the channel with a voltage-sensor toxin from spider venom, which is known to partition into the membrane, bind onto the channel, and alter its function (12, 13). Beyond the effects of lipid composition of the membrane, we discover that the membrane’s “mechanical state” exerts a prominent effect on both voltage-dependent gating and toxin interaction.

Membrane Influences Channel Gating and Pharmacology. Fig. 1 shows several basic properties of two apparently different Kv channels. Upon membrane depolarization the channels in Fig. 1A open (activate) very rapidly and then begin to undergo gradual closure while the membrane is still at the depolarized voltage (inactivation). Upon hyperpolarization the channels return to their closed conformation (deactivate). The activation phase upon depolarization is so rapid that the capacitive current associated with charging the membrane to its new voltage obscures the K⁺ current upstroke. In contrast to the fast activating channels, the Kv channels in Fig. 1B activate much more slowly and no inactivation is evident during the duration of the depolarized step. Other properties further distinguish the fast- (Fig. 1A) and slow- (Fig. 1B) activating channels. The midpoint voltage of the voltage-activation curve (voltage corresponding to half maximal activation) is –58 mV and 7 mV for fast- and slow-activating channels, respectively (Fig. 1C). The fast-activating channels are also sensitive to the tarantula venom toxin VSTx1 (Fig. 1D) whereas the slow-activating channels are insensitive (Fig. 1E).

The distinct behavior of two apparently different Kv channels described in Fig. 1 actually represent the very same channels functioning in different membranes. The Kv channel is called “paddle chimera,” a Kv1.2 channel with a voltage sensor paddle from Kv2.1 (14, 15). The properties of rapid activation, inactivation, a negative midpoint voltage and sensitivity to VSTx1 are observed when the channels are reconstituted into planar bilayers consisting of the lipids 1-palmitoyl-2-oleoyl-glycero-3-phosphoethanolamine (POPE) and 1-palmitoyl-2-oleoyl-glycero-3-phospho-1-glycerol (POPG) in a 3:1 ratio. The properties of slow activation, absence of inactivation, a midpoint voltage shifted by ≈60 mV, and insensitivity to VSTx1 are observed when the channels are expressed in the membranes of *Xenopus* oocytes.

Channels studied in planar bilayers first have to be synthesized in yeast cells and then purified in detergent, reconstituted into lipid vesicles and fused with the planar bilayer (15). Channels studied in oocyte membranes are synthesized by the oocytes after injection of RNA. To compare channels with similar histories we fused yeast-synthesized channels directly into oocyte membranes by injecting vesicles into the oocyte (Fig. 1F) (16). This maneuver enables a direct comparison of compositionally identical channels fused into cell membranes and planar bilayers. With respect to activation, inactivation, midpoint voltage and VSTx1 sensitivity currents measured in oocytes after RNA injection and after vesicle injection were indistinguishable (Fig. 1G–J). Therefore, the distinct channel properties observed in oocyte membranes and planar bilayers must

Author contributions: D.S. and R.M. designed research, performed research, analyzed data, and wrote the paper.

The authors declare no conflict of interest.

¹To whom correspondence should be addressed. E-mail: mackinn@rockefeller.edu.

This article contains supporting information online at www.pnas.org/cgi/content/full/0810187105/DCSupplemental.

© 2008 by The National Academy of Sciences of the USA

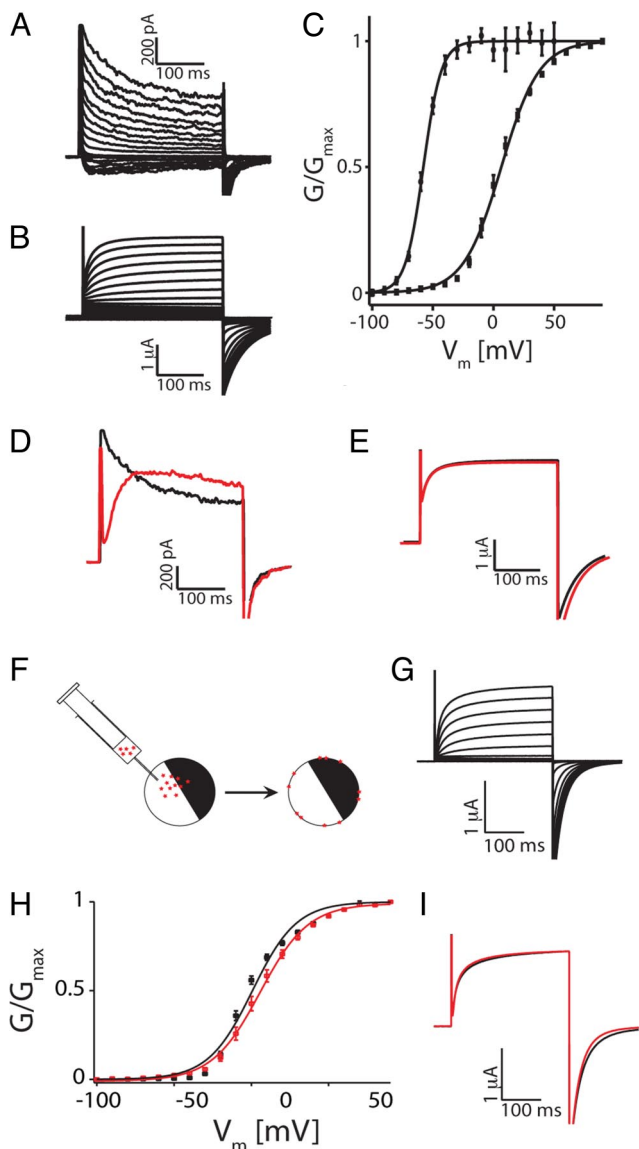


Fig. 1. The membrane regulates gating. (A) Paddle chimera in POPE:POPG vesicles was fused into POPE:POPG bilayers. Voltage pulses: holding potential (h.p.) -100 mV to 70 mV, $\Delta V = 10$ mV. (B) Oocytes expressing paddle chimera from mRNA in a 2-electrode voltage clamp (TEVC). Voltage pulses: h.p. -100 mV to 70 mV, $\Delta V = 10$ mV. (C) Boltzmann functions (solid lines) fit data (mean \pm SEM, $n = 13$) from A (filled circles) with $V_{0.5}$ (mV) and Z : -57.8 ± 0.4 , 3.4 ± 0.14 and data (mean \pm SEM, $n = 5$) from B (filled squares): 6.5 ± 0.5 , 1.6 ± 0.05 . (D) Paddle chimera in POPE:POPG bilayers, before (black) and after (red) addition of 500 nM VSTx1. Pulse from h.p. -100 mV to 70 mV. (E) Paddle chimera in oocytes in TEVC, before (black) and after (red) addition of $1 \mu\text{M}$ VSTx1. Pulse from h.p. -100 mV to 70 mV. (F) Diagram depicting the injection of reconstituted paddle chimera protein (red stars) into *Xenopus* oocytes. (G) Paddle Chimera vesicle injected oocytes in TEVC. Voltage pulses: h.p. -100 mV to 70 mV, $\Delta V = 10$ mV. (H) Boltzmann functions (solid lines) fit data (mean \pm SEM, $n = 5$) from B (filled circles) with $V_{0.5}$ (mV) and Z : 6.5 ± 0.5 , 1.6 ± 0.05 and data (mean \pm SEM, $n = 7$) from G (filled squares): 0.7 ± 1.2 , 1.7 ± 0.14 . (I) Paddle chimera vesicle injected oocytes in TEVC, before (black) and after (red) addition of $1 \mu\text{M}$ VSTx1. Pulse from h.p. -100 mV to 70 mV.

be due to environmental differences, either in the membrane or in the oocyte cytoplasm.

Effect of Membrane Lipid Composition. To evaluate the effect of lipid composition on function we produced planar bilayers from a lipid mixture that attempts to mimic the oocyte membrane (17). In the

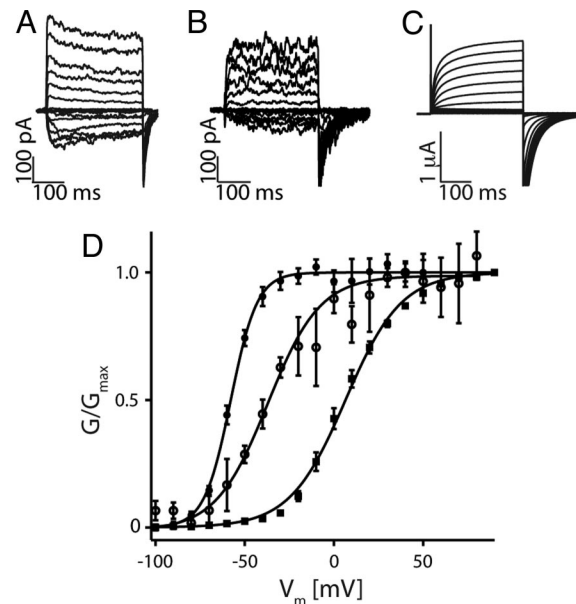


Fig. 2. The effect of lipid composition. Paddle chimera in POPE:POPG vesicles was fused into bilayers of POPE:POPG (A) or 1,2-dieicosenoyl-sn-glycero-3-phosphocholine:brain sphingomyelin:cholesterol (2:1:1) (B). CTX was used for capacitance transient subtraction in A and B. (C) Oocytes expressing paddle chimera from mRNA in a 2-electrode voltage clamp (TEVC). Voltage pulses (A–C): h.p. -100 mV to 70 mV, $\Delta V = 10$ mV. (D) Boltzmann functions (solid lines) fit data (mean \pm SEM, $n = 13$) from A (filled circles) with $V_{0.5}$ (mV) and Z : -57.8 ± 0.4 , 3.4 ± 0.14 , data (mean \pm SEM, $n = 3$) from B (open circles): -37.1 ± 1.9 , 1.7 ± 0.16 and data (mean \pm SEM, $n = 5$) from C (filled squares): 6.5 ± 0.5 , 1.6 ± 0.05 .

oocyte-like bilayers the Kv channels are more similar to channels in oocytes in that they do not inactivate (Fig. 2 A–C) and their voltage-activation curve is shifted to somewhat more positive voltages (Fig. 2D). However, the midpoint of activation is still not near that observed in oocytes. Of course we are not able to produce a genuine oocyte membrane mimic in the bilayer system for a number of reasons; oocyte membranes may have different lipid components in their inner and outer leaflets (i.e., they are asymmetric), many minor components of the oocyte membrane are still unknown, and our planar bilayers contain decane (18). It might seem reasonable to think that if we could accurately replicate the composition of an oocyte membrane then we would observe oocyte-like Kv function in the bilayer system. However, the experiments described below show that physical properties of the membrane other than lipid composition, which we categorize as the mechanical state, are also important to Kv channel function.

Effect of Membrane Mechanical State. Fig. 3 compares Kv channels in planar bilayers of POPE and POPG to Kv channels in oocyte membranes using whole cell recording and isolated membrane patches with different configurations. The Kv channels in isolated membrane patches (Fig. 3 B–E) exhibit properties that are intermediate between planar bilayers (Fig. 3A) and oocytes recorded in the whole cell mode (Fig. 3F). Moreover there is a graded response depending on the patch configuration. On-cell patches in the absence of negative pipette pressure and outside-out patches initially cause channels to be more oocyte-like in their behavior, whereas on-cell patches after application of negative pipette pressure, but not dependent on sustained maintenance of the pressure, and inside-out patches cause channels to exhibit more bilayer-like behavior. The response can be quantified using the midpoint voltage (Fig. 3G). In addition to the midpoint shift, there is a noticeable change in the slope of the activation curves: More negative midpoint voltages are associated with steeper activation

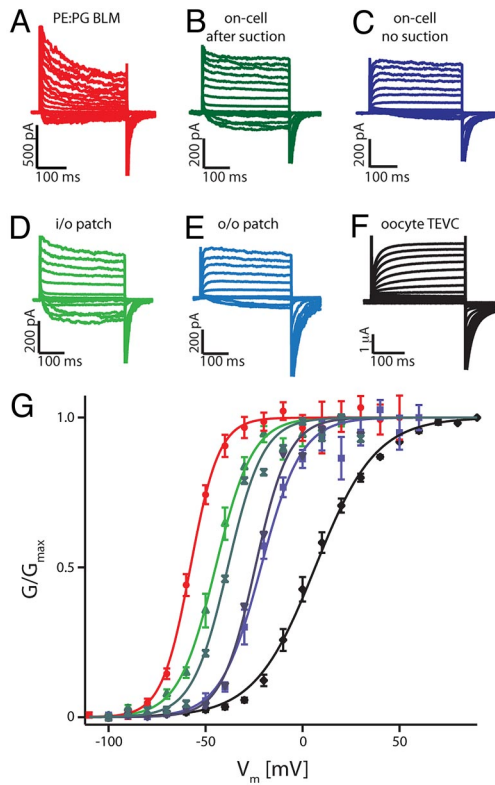


Fig. 3. The effect of membrane configuration. (A–F) Paddle chimera in various membrane configurations as denoted by the accompanying label. All voltage pulses h.p. -100 mV to 70 mV, $\Delta V = 10$ mV. (G) Boltzmann functions (solid lines) fit data (mean \pm SEM, $n = 4$ – 13 , except in B and C) from A (red) with $V_{0.5}$ (mV) and Z : -57.8 ± 0.4 , 3.4 ± 0.14 ; B (dark green): -38.6 ± 1 , 2.7 ± 0.27 ; C (dark blue): -24.4 ± 0.7 , 2.9 ± 0.2 ; D (light green): -44.8 ± 0.8 , 2.6 ± 0.19 ; E (light blue): -21.5 ± 1 , 2.4 ± 0.21 ; and F (black): 6.5 ± 0.5 , 1.6 ± 0.05 .

curves. The recordings in Fig. 3 B–E were made shortly after the formation of a gigaseal. Over a variable time channels in all patch configurations inevitably convert to gating properties similar to the inside-out patch, which is rather similar to the gating behavior observed in planar bilayers.

Closer Inspection of the Gating Conversion. Fig. 4 A–C shows that Kv channels in an outside-out patch can be converted rapidly from oocyte-like behavior to bilayer-like behavior by applying positive pressure inside the pipette. This effect is irreversible, meaning that once the positive pressure inside the pipette is returned to zero the gating behavior does not convert back. Therefore, the phenomenon we are describing here is distinct from reversible gating changes induced by pressure application to stretch-activated channels and voltage-dependent channels in membrane patches (9, 19, 20). Nevertheless, the conversion somehow seems most consistent with some change in the mechanical state of the membrane because it occurs essentially instantaneously upon application of pressure and because it occurs in on-cell patches in which communication with the cytoplasm is maintained.

Voltage-activation curves corresponding to three different stages during the conversion are shown (Fig. 4D). As pressure is applied the curves change in three respects: The midpoint voltage shifts to a more negative value, the slope increases, and the maximum amplitude increases. The midpoint voltage shift and slope increase are similar to differences in the curves shown in Fig. 3G. In Fig. 3G, data for each curve were obtained from a different patch, rendering a comparison of the amplitudes uninformative. For this reason the data in Fig. 3G have been normalized to unity. In Fig. 4D the data

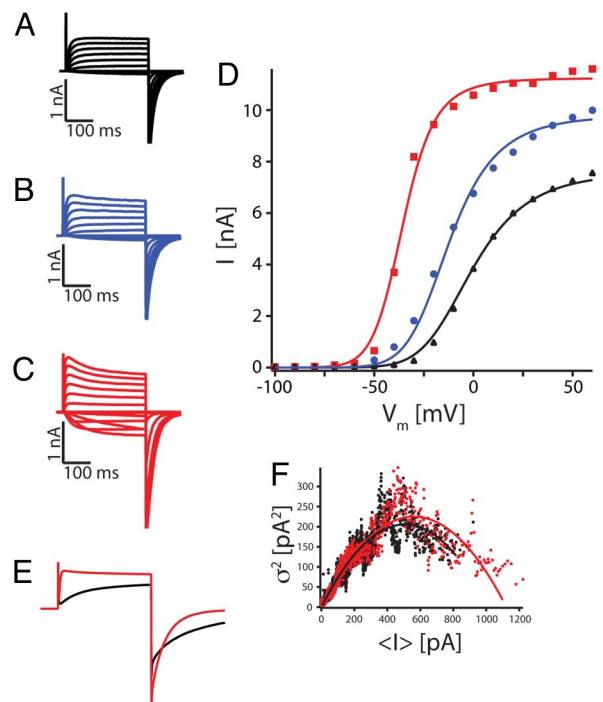


Fig. 4. The effect of membrane forces. Paddle chimera in the same outside-out patch with 0 mmHg (A, black), 5 mmHg (B, blue) and 15 mmHg (C, red) applied. Voltage pulses in A–C: h.p. -100 mV to 70 mV, $\Delta V = 10$ mV. (D) The solid curves are fit globally to the data from (A–C) with Eq. 4 (see *Modeling of Gating Conversion*) using the relationships $K_1(V) = K_1 \times \exp(z_1 \times V)$ and $I = (x \times P_o) : L(0 \text{ mmHg}) = 1.96 \pm 0.135$, $L(5 \text{ mmHg}) = 6.1 \pm 0.596$, $L(15 \text{ mmHg}) = 79.5 \pm 14.4$, $K_1 = 2.5 \pm 0.19$, $z_1 = 1.15 \pm 0.05$, $x = 11378 \pm 123$. (E) Average traces (50–60 sweeps each) of paddle chimera in the same outside-out patch for pulses from h.p. -100 mV to 50 mV. Applied pressure is 0 mmHg (black) and 15 mmHg (red). (F) Nonstationary Fluctuation analysis for patch data after 0 mmHg (black) and 15 mmHg (red) applied pressure. The solid curve is fit to the data with the relationship $\sigma^2 = i \times \langle I \rangle - \langle I \rangle^2 / N$ (see *Closer Inspection of the Gating Conversion*), with $i = 0.812 \pm 0.002$ pA and $N = 1,245 \pm 8$ channels for 0 mmHg (black) and $i = 0.802 \pm 0.003$ pA and $N = 1399 \pm 9$ channels for 15 mmHg (red).

were recorded from a single patch, thus the systematic increase in current amplitude is informative. The increased maximum amplitude could come about by any 1 or a combination of 3 possible occurrences: The single channel current (i) could increase, the number of channels in the patch (N) could increase, or the open probability (P_o) could increase. By analyzing the relationship between mean current $\langle I \rangle$ and variance σ^2 for channels in a membrane patch before and after conversion from oocyte-like behavior to bilayer-like behavior it is possible to determine the origin of the current increase through the expressions (21)

$$\langle I \rangle = N P_o i \tag{1}$$

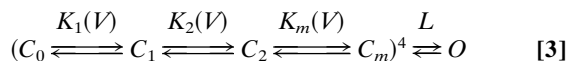
$$\sigma^2 = i \langle I \rangle - \frac{\langle I \rangle^2}{N} \tag{2}$$

This analysis shows that N and i remain approximately constant (the curves are nearly the same) while maximum P_o increases (data points extend to higher values of $\langle I \rangle$) (Fig. 4E and F). In the example shown, maximum P_o increased from 0.79 to 1.0 . Analysis of multiple patches shows that maximum P_o increases from a range 0.6 to 0.8 initially to >0.9 when channels convert from oocyte-like to bilayer-like gating behavior in a patch. In summary, three changes in the voltage-activation curve occur when the channels convert: The midpoint voltage shifts negative, opening becomes a steeper function of membrane voltage, and a higher maximum P_o is achieved.

These gating effects are not unique to the paddle chimera channel. The *Shaker* Kv channel, for example, undergoes a similar conversion following patch excision from the oocyte surface [supporting information (SI) Fig. S1].

Modeling the Gating Conversion. Kinetic and equilibrium studies of Kv channel gating show that upon membrane depolarization a channel undergoes multiple transitions during its sojourn from a closed state to the open state (22, 23). Most of the voltage dependence occurs in the early kinetic transitions, before pore opening, and then eventually the pore opens in a concerted manner. Atomic structures of Kv channels are entirely consistent with this kinetic description (14, 24, 25). The structures reveal 4 voltage sensors disposed as nearly independent domains surrounding the pore, suggesting that conformational changes can occur within each voltage sensor independently. Four S4–S5 linker helices, which attach the voltage sensors to the pore, are positioned as if to constrict the pore when the voltage sensors are in their closed “hyperpolarized conformation.” Presumably when the 4 voltage sensors achieve their “depolarized conformation” the S4–S5 linker helices move, enabling the pore to undergo a concerted (all 4 subunits simultaneously) transition from the closed to opened conformation.

A simple state diagram captures this description (26):



Here, m transitions must occur within each of 4 independent voltage sensors before the pore can open. Voltage-dependent equilibrium constants $K_i(V)$ characterize conformational transitions within the voltage sensors, the equilibrium constant L characterizes the conformational transition of the pore from closed to open. The open probability is given by (26):

$$P_o = \frac{L \left(\prod_{i=1}^m K_i(V) \right)^4}{\left(1 + \sum_{n=1}^m \prod_{i=1}^n K_i(V) \right)^4 + L \left(\prod_{i=1}^m K_i(V) \right)^4} \quad [4]$$

Using the simplest realization of this model, in which the voltage-dependent conformational changes within each subunit are grouped into a single voltage-dependent transition ($m = 1$) and L is voltage-independent, we can account for the 3 curves in Fig. 4D by adjusting a single parameter L . Recall that these curves differ in three quantitative aspects: midpoint voltage, steepness, and maximum P_o . All three aspects are satisfied simultaneously through adjustment of L , but not $K_i(V)$. The same model with L as the sole adjusted parameter also accounts for the *Shaker* Kv channel data (Fig. S1, solid curves). Thus, it would appear that “conversion” represents a condition under which the pore-opening transition is more highly favored.

Membrane Dependence of Voltage Sensor Toxin Activity. The most puzzling initial observation in this study concerns the dependence of VSTx1 sensitivity on the membrane: Channels are sensitive to this toxin in planar bilayers but insensitive in oocytes (Fig. 1D and E). VSTx1 and other voltage sensor toxins partition into the membrane to modify Kv channel gating (12, 27). Moreover, the type of lipid in the membrane is known to influence the partition coefficient and therefore one might expect lipid compositional differences to be at the root of the differential VSTx1 sensitivity in the two different membrane systems (12, 28). Against expectation, experiments show that

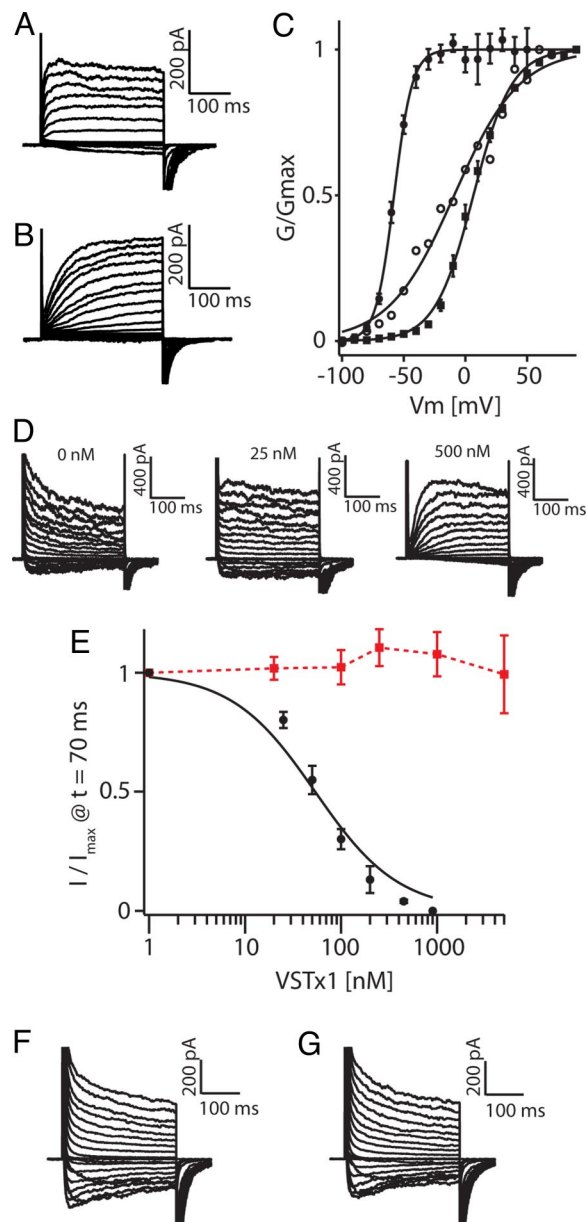


Fig. 5. Membrane mechanics and voltage sensor toxins. All voltage pulses from h.p. -100 mV to 70 mV, $\Delta V = 10$ mV. (A and B) Paddle chimera in an outside-out patch, before (A) and after (B) addition of 500 nM VSTx1. (C) Boltzmann functions (solid lines) fit data (mean \pm SEM, $n = 5$ – 13 , except data from B) from A (filled circles) with $V_{0.5}$ (mV) and Z : -57.8 ± 0.4 , 3.4 ± 0.14 , data from B (open circles) with $V_{0.5}$ (mV) and Z : -9.1 ± 2 , 0.9 ± 0.07 and data from Fig. 1B (filled squares) with $V_{0.5}$ (mV) and Z : 6.5 ± 0.5 , 1.6 ± 0.05 . (D) Paddle chimera in POPE:POPG bilayers. VSTx1 was added to the indicated concentration. (E) VSTx1 affinity titration with Paddle chimera (black circles) and Kv1.2 channels (red squares) in POPE:POPG bilayers. Fraction of residual current I/I_{\max} (mean \pm SEM, $n = 3$) at $t = 70$ ms after depolarization is graphed as a function of $\log(\text{VSTx1 concentration})$. The solid line represents a fit to the titration data with $I/I_{\max} = (1 + [\text{VSTx1}]/K_d)^{-1}$ with $K_d = 54 \pm 8.8$ nM. (F and G) Kv1.2 in POPE:POPG bilayers, before (F) and after (G) addition of 500 nM VSTx1.

VSTx1 sensitivity is in fact dependent upon the mechanical state of the membrane (Fig. 5). When applied to channels in an outside-out patch from oocytes VSTx1 causes a slowing of activation (Fig. 5A and B) similar to the effect observed in planar bilayers (Fig. 1D). The kinetic changes are also associated with a shift in the midpoint voltage to more positive values (Fig. 5C).

Insensitivity of the paddle chimera channel to VSTx1 applied

to whole oocytes cannot be attributed to an inability of the toxin to reach the oocyte surface: VSTx1 does not affect paddle chimera channels recorded in whole cell mode in devittellinized oocytes (data not shown) and the pore-blocking toxin CTX, which is similar in size to VSTx1, inhibits the paddle chimera channel in whole oocytes and in planar lipid bilayers with similar affinities (Fig. S2). Furthermore, Swartz and colleagues have shown that in whole oocytes VSTx1 inhibits a chimera Kv2.1 channel containing the KvAP voltage sensor paddle (29). Therefore, VSTx1 must be able to reach the oocyte surface.

The apparent affinity of VSTx1 for paddle chimera in excised membrane patches and in planar bilayers is high, as it exerts its effect in the 10 to 50 nM range (Fig. 5 D and E). Molecular specificity is also an essential component of the VSTx1-paddle chimera interaction: VSTx1 does not affect Kv1.2 in planar bilayers (Fig. 5 F and G). Paddle chimera and Kv1.2 differ only in the amino acid composition of the voltage sensor paddle, which has been shown to form the binding site for voltage sensor toxins (30, 31).

Apparent high affinity and molecular specificity distinguish in a fundamental manner the VSTx1-paddle chimera interaction from the previously reported GsMTx4-stretch-activated channel interaction (32). GsMTx4 modifies stretch-activated channel gating with low affinity (500 nM range) and in the absence of traditional molecular specificity, as the D-enantiomeric form of the toxin was reported to be as effective as the L-enantiomer (32). Amphipathic, membrane active molecules such as capsaicin have been shown to alter gating of voltage-dependent Na⁺ (Nav) channels. These agents exert their effects in the 10 μM range and can be mimicked by detergents (33). In contrast to low-affinity amphipathic agents acting on Nav channel gating and GsMTx4 acting on stretch-activated channels, VSTx1 functions at low concentration, exhibits molecular specificity mediated by the protein surface of the voltage sensor paddle, and yet it is sensitive to the mechanical state of the membrane.

Discussion

The functional characteristics of Kv channels can depend on both the lipid composition and the mechanical state of the membrane. When comparing the paddle chimera channel in whole *Xenopus* oocytes and in planar bilayers formed from POPE and POPG we conclude that lipid compositional differences account for modest changes in function, somewhat similar in magnitude to the effects of lipid head group modifying lipases on various Kv channels expressed in *Xenopus* oocytes (10). The conversion of gating and pharmacological properties as a consequence of patch formation on glass electrodes shows that the influence of the membrane's mechanical state on function are large.

In all patch configurations, even on-cell in which continuity of the patch's internal face is maintained with the cytoplasm, the gating properties eventually convert to bilayer-like. Although it is possible that the conversion results from an alteration of signaling factors operating on the cytoplasmic face of the channel, we think that this explanation is unlikely for the following reason: the effect can be made to occur essentially instantaneously by application of a pressure difference across the patch. In Fig. 4 A–D the pressure-induced conversion is demonstrated for the case of an excised outside-out patch in which communication with the cytoplasm, by virtue of outside-out seal formation, was terminated before any pressure application. By applying pressure, and thus force to the patch, a fundamental change in the channel's behavior is elicited, which we attribute to some mechanical property of the patch.

The pressure-induced changes described here are distinct from published accounts of reversible pressure-induced changes in channel gating. Here, the change is inevitable even in the absence of pressure; pressure application merely speeds the process. Here, the change is irreversible upon removal of pres-

sure, which would seem to imply an irreversible change in the membrane or channels. Other irreversible effects on channel gating have been reported. For example the rate of Na⁺ channel inactivation is changed irreversibly upon transient application of pressure (34, 35). One possible explanation for irreversible gating changes could be that cytoskeleton attachments to the membrane are disrupted. If this were the case, it would be interesting because it would mean that the cytoskeleton is able to influence the membrane in such a way as to have profound effects on the function of a channel.

Lipid membranes in planar bilayers and glass electrodes are mechanically different from intact cell membranes in other respects independent of cytoskeleton. Past studies indicate that planar bilayers and membrane patches on glass pipettes are both under tension even in the absence of a pressure gradient. Work by Haydon and colleagues (36, 37) estimated the tension of phosphatidylcholine bilayers with decane to be in the range of 3–5 mN/m. Webb and colleagues measured the line adhesion tension on membrane patches in glass pipettes and showed that its value is variable, ranging from 0.5 to 4 mN/m, depending on the specific patch (38). They attribute the source of this tension to adhesion forces between the lipid membrane and glass. The source of membrane tension in both these systems probably originates in the boundary. In a planar bilayer the boundary is formed by the torus of lipid and solvent and perhaps the solid support surrounding the bilayer. In a patch pipette the boundary is formed by lipid adhering to the glass at the patch perimeter. By contrast, large membrane vesicles unrestrained by boundaries can have very low tensions (< 10⁻² mN/m) (39, 40). Likewise, the tension of cell membranes under normal physiological conditions is near zero (41, 42). Cell membranes typically have “excess membrane” in the form of folds and invaginations. This is particularly true of stage VI *Xenopus* oocyte membranes, in which electrical capacitance measurements show that the actual membrane area is approximately ten times greater than the area calculated on the basis of the oocyte radius (data not shown).

If the Kv channels are sensitive to the differences in tension intrinsic to planar bilayers and membrane patches then tension in the membrane could account for the gating differences we observe. The conversion from oocyte-like to bilayer-like behavior might reflect the development of adhesive forces between the lipid and glass, which would be irreversible. Through fitting of Eq. 4 to the data in Fig. 4 we show that conversion corresponds to—or at least can be accounted for by—a shift in the pore-opening equilibrium toward the open conformation. Crystal structures of closed and opened K⁺ channels show that that upon opening the pore expands its cross-sectional area in the membrane's inner leaflet. Thus, in a higher tension membrane the open conformation will be favored. Further experiments involving direct measurement of membrane tension will be necessary to test this tension hypothesis.

How can we explain voltage sensor toxin sensitivity being a function of the mechanical state of the membrane? At present we have insufficient data to understand this very surprising observation. However, we are intrigued by an obvious feature of the data: VSTx1-inhibited channels in planar bilayers and patches on glass electrodes actually appear similar in behavior to channels recorded from whole oocytes (Fig. 1 A, B, and D). VSTx1 inhibited channels in planar bilayers, for example, exhibit slow activation, little inactivation, and the midpoint voltage is shifted toward positive voltages (Figs. 1 D and 5 D). These features are all qualitatively similar to paddle chimera channels in whole oocytes. On the basis of these observations we put forth the following hypothesis, which is to be tested with future experiments. The hypothesis is this: Voltage sensor toxins modify gating by altering the forces acting between the channel and the membrane. Consequently, the effect that the toxin will have on a channel will depend on the channel-membrane forces, which will be a function of the lipid composition and the

mechanical state. In essence our hypothesis posits that the voltage sensor toxin VSTx1 is not a conventional “allosteric regulator” that stabilizes a particular state of the channel through a protein–protein interaction, but rather it alters channel function by perturbing interactions between the channel and membrane.

Voltage sensor toxins were first thought to be allosteric modifiers that bind to voltage sensors through protein–protein interactions that determine their molecular specificity (30, 31). That original view was then modified to include the concept that voltage sensor toxins partition into the membrane to gain access to their binding site on the voltage sensor paddle and increase their local concentration near the channel (12, 27). The findings presented here suggest that the reason for membrane partitioning may be more than site access and local toxin concentration. We suspect that the fundamental mechanism of VSTx1 action is connected to its ability to modify membrane forces experienced by the ion channel, and to modify membrane forces VSTx1 must partition into the membrane.

Methods

Protein Preparation and Reconstitution. Paddle chimera protein (α and β 1 subunits) was expressed, purified and reconstituted as described in ref. 15.

Electrophysiology. Whole oocyte recordings. mRNA encoding the paddle chimera protein α subunit was prepared by T7 polymerase transcription and injected into *Xenopus laevis* oocytes. Reconstituted paddle chimera protein in POPE:POPG 3:1 (m/m) vesicles was dialyzed against 100 mM KCl, 10 mM Hepes-KOH pH 7.4 for 2 h and injected into *Xenopus laevis* oocytes. K⁺ currents were recorded under 2-electrode voltage clamp (OC725C; Warner Instrument) 1–2 days after mRNA injection or 12–24 h after vesicle injection.

1. Dowhan W (1997) Molecular basis for membrane phospholipid diversity: Why are there so many lipids? *Annu Rev Biochem* 66:199–232.
2. van Meer G, Voelker DR, Feigenson GW (2008) Membrane lipids: Where they are and how they behave. *Nat Rev Mol Cell Biol* 9:112–124.
3. Marheineke K, Grünewald S, Christie W, Reiländer H (1998) Lipid composition of *Spodoptera frugiperda* (Sf9) and *Trichoplusia ni* (Tn) insect cells used for baculovirus infection. *FEBS Lett* 441:49–52.
4. Renkonen O, Gahmberg CG, Simons K, Kääriäinen L (1972) The lipids of the plasma membranes and endoplasmic reticulum from cultured baby hamster kidney cells (BHK21). *Biochim Biophys Acta* 255:66–78.
5. Robinson NC (1993) Functional binding of cardiolipin to cytochrome c oxidase. *J Bienerg Biomembr* 25:153–163.
6. Schmidt D, Jiang QX, Mackinnon R (2006) Phospholipids and the origin of cationic gating charges in voltage sensors. *Nature* 444(7120):775–779.
7. Valiyaveetil FI, Zhou Y, Mackinnon R (2002) Lipids in the structure, folding, and function of the KcsA K⁺ channel. *Biochemistry* 41:10771–10777.
8. Oliver D, et al. (2004) Functional conversion between A-type and delayed rectifier K⁺ channels by membrane lipids. *Science* 304:265–270.
9. Perozo E, Kloda A, Cortes DM, Martinac B (2002) Physical principles underlying the transduction of bilayer deformation forces during mechanosensitive channel gating. *Nat Struct Biol* 9:696–703.
10. Ramu Y, Xu Y, Lu Z (2006) Enzymatic activation of voltage-gated potassium channels. *Nature* 442:696–699.
11. Hille Bertil (2001) *Ion Channels of Excitable Membranes* (Sinauer Associates, Sunderland, MA).
12. Lee SY, Mackinnon R (2004) A membrane-access mechanism of ion channel inhibition by voltage sensor toxins from spider venom. *Nature* 430:232–235.
13. Ruta V, Jiang Y, Lee A, Chen J, Mackinnon R (2003) Functional analysis of an archaeobacterial voltage-dependent K⁺ channel. *Nature* 422:180–185.
14. Long SB, Tao X, Campbell EB, Mackinnon R (2007) Atomic structure of a voltage-dependent K⁺ channel in a lipid membrane-like environment. *Nature* 450:376–382.
15. Tao X, Mackinnon R (2008) Functional analysis of Kv1.2 and paddle chimera Kv channels in planar lipid bilayers. *J Mol Biol* 382:24–33.
16. Morales A, et al. (1995) Incorporation of reconstituted acetylcholine receptors from Torpedo into the *Xenopus* oocyte membrane. *Proc Natl Acad Sci USA* 92:8468–8472.
17. Hill WG, et al. (2005) Isolation and characterization of the *Xenopus* oocyte plasma membrane: A new method for studying activity of water and solute transporters. *AJP Renal Physiology* 289:F217–F224.
18. Miller C (1986) *Ion Channel Reconstitution* (Plenum, New York).
19. Laitko U, Juranka PF, Morris CE (2006) Membrane stretch slows the concerted step prior to opening in a Kv channel. *J Gen Physiol* 127:687–701.
20. Sukharev SI, Sigurdson WJ, Kung C, Sachs F (1999) Energetic and spatial parameters for gating of the bacterial large conductance mechanosensitive channel, MscL. *J Gen Physiol* 113:525–540.
21. Sigworth FJ (1980) The variance of sodium current fluctuations at the node of Ranvier. *J Physiol (London)* 307:97–129.

Electrodes were drawn from borosilicate glass capillaries (VWR) and filled with 3 M KCl. Oocyte bath solution contained: 98 mM KCl, 0.3 mM CaCl₂, 1 mM MgCl₂, and 5 mM Hepes-KOH (pH 7.4). Analog data from the amplifier were filtered (1kHz) using the built-in 4-pole Bessel filter, digitized at 10kHz (Digidata 1440A; Molecular Devices) and stored on a computer hard-disk.

Patch clamp recordings. K⁺ currents were recorded in on-cell, inside-out and outside-patches from oocytes 5–6 days after mRNA injection. Electrodes were drawn from borosilicate patch glass (VWR) and polished (MF-83, Narishige) to a resistance of 0.8–1.2 M Ω . For all patch configurations the extracellular solution contained (mM): 100 KCl, 2 MgCl₂, 5 Hepes-KOH pH 7.4 and the intracellular solution contained (mM): 100 KCl, 1 EGTA, 5 Hepes-KOH pH 7.4. The analog signals were filtered (1kHz) using the built-in 4-pole Bessel filter of an Axopatch 200B patch clamp amplifier (Molecular Devices) in patch-mode, digitized at 10 kHz (Digidata 1440A, Molecular Devices) and stored on a computer hard-disk, except for the nonstationary fluctuation analysis experiments, for which the analog signals were filtered at 5kHz and digitized at 20kHz. Patch pressure was generated using water-filled U-shaped tubing connected to atmospheric pressure and applied via the patch pipette sideport. The pressure was monitored using an in-line manometer (Sper Scientific).

Planar lipid bilayer recordings. Bilayer experiments followed the procedures in refs. 15 and 18. Bilayers were formed over a 300- μ m hole in a polystyrene partition that separated two aqueous chambers. After vesicles with channels were fused into the bilayer, voltage-clamp measurements in whole-cell mode were made.

ACKNOWLEDGMENTS. We thank Alice L. MacKinnon (The Rockefeller University) for providing CTX and VSTx1 and Xiao Tao (The Rockefeller University) for providing the paddle chimera mRNA and Stanislas Leibler, Evan Evans, and Rob Phillips for helpful discussions. This work was supported by National Institutes of Health Grant GM43949. D.S. is supported by the Boehringer Ingelheim Fonds. R.M. is an Investigator in the Howard Hughes Medical Institute.

22. Hoshi T, Zagotta WN, Aldrich RW (1994) Shaker potassium channel gating. I: Transitions near the open state. *J Gen Physiol* 103:249–278.
23. Schoppa NE, Sigworth FJ (1998) Activation of Shaker potassium channels. III. An activation gating model for wild-type and V2 mutant channels. *J Gen Physiol* 111:313–342.
24. Long SB, Campbell EB, Mackinnon R (2005) Crystal structure of a mammalian voltage-dependent Shaker family K⁺ channel. *Science* 309:897–903.
25. Long SB, Campbell EB, Mackinnon R (2005) Voltage sensor of Kv1.2: Structural basis of electromechanical coupling. *Science* 309:903–908.
26. Yifrach O, Mackinnon R (2002) Energetics of pore opening in a voltage-gated K(+) channel. *Cell* 111:231–239.
27. Milescu M, et al. (2007) Tarantula toxins interact with voltage sensors within lipid membranes. *J Gen Physiol* 130:497–511.
28. Jung HJ, et al. (2005) Solution structure and lipid membrane partitioning of VSTx1, an inhibitor of the KvAP potassium channel. *Biochemistry* 44:6015–6023.
29. Alabi AA, Bahamonde MI, Jung HJ, Kim JI, Swartz KJ (2007) Portability of paddle motif function and pharmacology in voltage sensors. *Nature* 450:370–375.
30. Swartz KJ, Mackinnon R (1997) Hanatoxin modifies the gating of a voltage-dependent K⁺ channel through multiple binding sites. *Neuron* 18:665–673.
31. Swartz KJ, Mackinnon R (1997) Mapping the receptor site for hanatoxin, a gating modifier of voltage-dependent K⁺ channels. *Neuron* 18:675–682.
32. Suchyna TM, et al. (2004) Bilayer-dependent inhibition of mechanosensitive channels by neuroactive peptide enantiomers. *Nature* 430:235–240.
33. Lundbaek JA (2008) Lipid bilayer-mediated regulation of ion channel function by amphiphilic drugs. *J Gen Physiol* 131:421–429.
34. Scherbatko A, Ono F, Mandel G, Brehm P (1999) Voltage-dependent sodium channel function is regulated through membrane mechanics. *Biophys J* 77:1945–1959.
35. Tabarean IV, Juranka P, Morris CE (1999) Membrane stretch affects gating modes of a skeletal muscle sodium channel. *Biophys J* 77:758–774.
36. Cook G, Redwood W, Taylor A, Haydon D (1968) The molecular composition of black hydrocarbon films in aqueous solutions. *Colloid Polymer Sci* 227:28–37.
37. Requena J, Brooks DE, Haydon D (1977) van der Waals forces in oil/water systems. *J Colloid Interf Sci* 58:26–35.
38. Opsahl LR, Webb WW (1994) Lipid-glass adhesion in giga-sealed patch-clamped membranes. *Biophys J* 66:75–79.
39. Kwok R, Evans E (1981) Thermoelasticity of large lecithin bilayer vesicles. *Biophys J* 35:637–652.
40. Rawicz W, Olbrich KC, McIntosh TJ, Needham D, Evans E (2000) Effect of chain length and unsaturation on elasticity of lipid bilayers. *Biophys J* 79:328–339.
41. Dai J, Sheetz MP, Wan X, Morris CE (1998) Membrane tension in swelling and shrinking molluscan neurons. *J Neurosci* 18:6681–6692.
42. Wolfe J, Steponkus PL (1983) Mechanical properties of the plasma membrane of isolated plant protoplasts: Mechanism of hyperosmotic and extracellular freezing injury. *Plant Physiol* 71:276–285.